Acknowledgment

I would like to express my sincere thanks and deep appreciation to my supervisors, **Dr. Sabah M. Juma** for suggesting the present project, supervision, and valuable discussions and **Dr. Fatin Abdul Jalil Al-Mudarris** for completing the superviand encouragement throughout the period of this work.

I am grateful to the Dean of College of Science and the staff of the Department of Physics at Al-Nahrain University for their valuable support and cooperation.

The assistance given by **Mr. Ibrahim A. M.Sadiq** and **Ms. Basma H. H. Al-Shammary** is highly appreciated.

Finally, I would like to express my appreciation with high gratitude and deep to my family.

Ali

DEDICATION TO MY FAMILY

Certification

We certify that this thesis entitled **"A Computational Investigation on Some Properties of a Gabor Lens"** is prepared by **Mr. Ali Ismail Mohammed Al-Smawi** under our supervision at the College of Science of Al-Nahrain University in partial fulfillment of the requirements for the degree of **Master of Science in Physics.**

Supervisor: Prof. Dr.Sabah M.Juma
Date: / /2006

Supervisor:Dr.Fatin.Al-Mudarris
Date: / /2006

In view of the recommendations, we present this thesis for debate by the examination committee.

Dr. Ahmad K. Ahmad
Head of Physics Department
Date:

Examination Committee Certification

We certify that we have read the thesis entitled **"A Computational Investigation on Some Properties of a Gabor Lens"** and as an examination committee, examined the student **Mr Ali Ismail Mohammed Al-Smawi** on its contents, and that in our opinion it is adequate for the partial fulfillment of the requirments of the degree of **Master of Science in Physics.**

Signature:
Name: Ali H. Hassan
Title :(Member)
Date: / /2006

Signature:
Name:Shatha M. Al Hilly
Title: (Member)
Date: / /2006

Signature:
Name:Ahmad K. Ahmad
Title: (Chair man)
Date: / /2006

Signature:
Name:Dr.Fatin.Al-Mudarris
Title :(supervisor)
Date: / /2006

Signature:
Name:Dr. Laith Abdul Aziz Al-Ani

(Dean of the College of science)
Date: / /2006

Republic of Iraq
Ministry of Higher Education and Scientific Research
AL-Nahrain University
College of Science
Physics Department

A Computational Investigation on Some Properties of a Gabor Lens

A Thesis
Submitted to the College of Science of
Al-Nahrain University in Partial Fulfillment of
the Requirements for the Degree of

Master of Science

In

Physics

By

Ali Ismail Mohammed Al-Smawi
(B.Sc. 2003)

in

Jumadi el akher1427 A.H. **July 2006 A.D.**

جمهورية العراق
وزارة التعليم العالي والبحث العلمي
جامعة النهرين
كلية العلوم
قسم الفيزياء

دراسة حاسوبية عن بعض خواص عد سة گابور

رسالة
مقدمة إلى كلية العلوم في جامعة النهرين
وهي جزء من متطلبات نيل درجة ماجستير في

الفيزياء

من قبل

علي اسماعيل محمد السماوي
(*بكلوريوس* ٢٠٠٣)

في

جمادى الاخر ١٤٢٧هـ 2006A.D.تموز

Synopsis

A computational investigation has been carried out in some properties of Gabor lens with the aid of personal computer under the absence of space-charge effects. This work has been concentrated on designing two concentric, electrostatic and magnetic lenses. Electrostatic lens is a two-electrode immersion lens whose electrodes are cylindrical in shape separated by a separation distance. Magnetic lens is a number of turns of the current-carrying coil of a hypothetical rectangular field of length L. The variable parameters of the electrostatic lens are the voltage ratio and the separation distance while in the magnetic lens the variable are the Ampere-turn and lens length. The combined electrostatic and magnetic lens (Gabor lens) has been investigated under zero and infinite magnification conditions. The paraxial ray equation has been solved with the aid of the axial electric and magnetic potential distribution using Runge-Kutta method. The axial potential and its first and second derivatives have been used for computing the optical properties of the lens under consideration. The lens spherical and chromatic aberration coefficients have been normalized in term of the focal length under zero and infinite magnification conditions.

المستخلص

لقد جرت دراسة حاسوبية لبعض خواص عدسة گابور و بمساعدة الحاسوب الشخصي في حالة عدم وجود تاثير لشحنة الفراغ. لقد تركز العمل على تصميم عدستين كهروسكونية و مغناطيسية متحدة المركز. العدسة الكهروسكونية هي عدسة ثنائية الاقطاب مغمورة و اقطابها لها شكل اسطواني تفصلهما مسافة **s**. العدسة المغناطيسية هي عبارة عن ملف يمر به تيار يتكون من عدد من اللفات ذات مجال مستطيل و طول L. ان متغيرات العدسة الكهروسكونية هي النسبة بين الاقطاب و المسافة بينهما، بينما في العدسة المغناطيسية فكانت عدد اللفات-التيار و طول العدسة. العدسة المركبة من العدسة الكهروسكونية و العدسة المغناطيسية (عدسة گابور) تم دراستها عندما تعمل تحت ظروف التكبير الصفر و المالانهائي. تم حل معادلة المسار المحورية بمساعدة توزيع المجال الكهربائي و المغناطيسي المحوري و باستعمال طريقة رنج-كوتا. استعمل المجال المحوري ومشتقتيه الاولى و الثانية لحساب الخواص البصرية للعدسة. ان معاملي الزيغ الكروي واللوني تم معايرتها بالنسبة الى البعد البؤري للعدسة و لظروف التكبير الصفري واللانهائي.

References

EL-Kareh, A.B., and EL-Kareh, J.C.J. (1970)
Electron Beams, Lenses and Optics, Vol.2,
(Academic Press, New York and London)

Gabor.D (1947)
A Space-Charge Lens for the Focusing of Ion Beams
Nature **160**, 89-90

Goncharov , Alexey A., Ivan M. Protsenko (2000)
Manipulating Large-Area, Heavy Metal Ion Beams with a High-Current Electrostatic Plasma Lens
IEEE, Vol.**28**, no.6, 2238-2246

Hamad, B.H. (2003)
Design of an Electrostatic Lens Using the Charge Density Method
M.S.c. Thesis, Al-Nahrain University, Baghdad, Iraq

Hawkes P. W. (1972)
Electron Optics and Electron Microscopy
(Academic Press, London)

Hawkes P. W. (1982)
Magnetic Electron Lenses
(Springer-Verlag, London)

Hawkes, P.W., and Kasper, E. (1989)
*Principles of Electron Optics, Vol.**1**,*
(Academic Press, New York)

Ivanov B.I. (2004)
Plasma Focusing Devices in External Programmed Magnetic Field
NSC KIPT, Kharkov, Ukraine
www.cern.ch

Klemperer, O., and Barnett (1971)
Electron Optics
(Cambridge University Press, London)

Kuffel, E. and Abdullah, A. (1979)
High-Voltage Engineering
(Pergamon Press, Oxford)

Maloff,I.G., Epstein,D.W (1938)
Electron Optics in Television
(McGraw-Hill Book Company, New York and London)

Meusel,O., Pozimski,J., Jakob, A., Gabor, C., and **Ratzinger,U. (2001)**
Progress in Gabor Lens Development
Annual Report HEDIM, p.25
Institut für Angewandte physic der Johann Wolfgang Goethe, Frankfurt, Germany

Morozov, A., (1965)
Focusing of cold quasineutral beams in electromagnetic fields
Dokl.Acad.Nauk USSR, vol.**163**, no.6, 1363-1366

Munro, E. (1975)
A set computer programs for calculating the properties of electron lenses
Department of Engineering Report CUED/B –Elect TR45,
University of Cambridge,UK

Myers,L.M (1939)
Electron Optics, Theoretical and Practical
(Chapman & Hall Press, London)

Palkovic.J.A (1989)
Gabor Lens Focusing of a Negative Ion Beam
IEEE, PAC 1989, 304-306

Reiser (1989)
Comparison of Gabor Lens, Gas Focusing and Electrostatic Quadrupole Focusing for Low Energy Beams
Proc. PAC, Chicago, USA

Rempfer, G.F. (1990)
A Theoretical Study of the Hyperbolic Electron Mirror as a Correcting Element for Spherical and Chromatic Aberration in Electron Optics
J.Appl.Phys, **67**, 6027-6040

Rempfer, G.F. and Griffith, O.H.(1992)
Emission Microscopy and Related Techniques: Resolution in Photo-Electron Microscopy, Low Energy Electron Microscopy and Mirror Electron Microscopy
Ultramicroscopy, **47**, 35-57

Szilagyi, M., Szep, J., and Lugosi, E.(1987)
A Systematic Analysis of Two-Electrode Electrostatic Lenses
IEEE Trans.**ED-34**, 1848-1857

Contents

1. GABOR LENS

1.1 Introduction

When a particle beam propagates through background gas, plasma is formed by collisional ionization resulting in (partial) neutralization of the beam's space charge. This "gas focusing" effect occurs naturally and often utilized for improving high-current beam transport. Gabor, in 1947, proposed a non-neutral electron plasma confined in a magnetron-type trap as effective "space-charge lens" for positive ion beams. This "Gabor lens", which offers better control and focusing strength than both gas focusing and applied fields, has been investigated by several research groups since its invention **[Reiser 1989].**

A Gabor lens is a charged particle lens which may be useful for matching an ion beam into a radio frequency quadrupole (RFQ). It is also interesting from a purely physical perspective since it contains non-neutral plasma. Focusing an ion beam with a given sign of charge in a Gabor lens requires a non-neutral plasma with the opposite sign of charge of the beam. The electric field in the Gabor lens provides the external forces to focus the beam ions **[Gabor 1947].**

1.2 Gabor Lens Construction

The design concept of a Gabor lens for an electron beam is illustrated somewhat simplistically in figure 1.1. There is a small opposition coil at one end of the lens to create a cusp in the magnetic field. This gives the plasma hydromagnetic stability. It is necessary to place an iron shell around the lens to shield the source from the magnetic

field of the lens. The advantage of this configuration is that the electrons emitted by the cathode are born in a region with B=0, i.e., their canonical angular momentum P is zero **[Reiser 1989].**

In the design shown in figure 1.1, a magnetic field is produced by two coils of uneven length, in opposition. A hot cathode in the form of a circular loop is arranged at or near the magnetic field-line which crosses the axis. This arrangement is necessary, as electrons which have to cross magnetic flux lines are prevented by their angular momentum from reaching the axis **[Gabor 1947].**

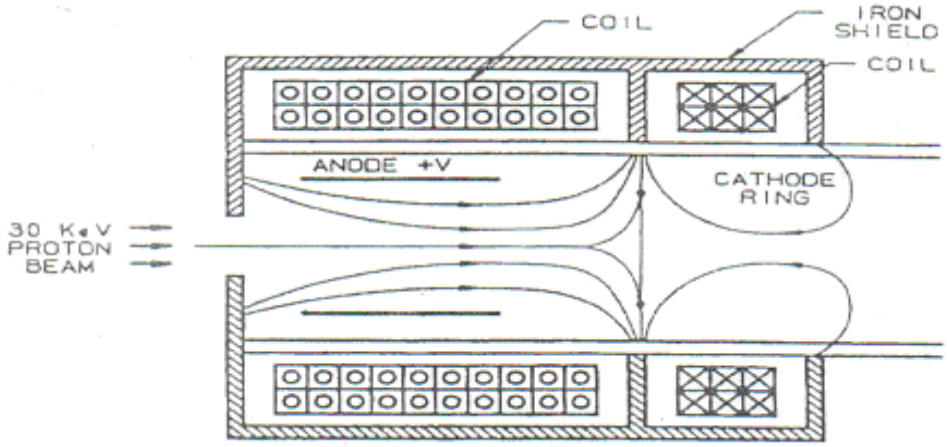

Figure 1.1. Gabor lens with magnetic field cusp. The cusp adds stability of the plasma **[J.A.Palkovic 1989].**

In the region where the magnetic field is approximately axial and homogeneous, a cylindrical electrode, the 'anode ', is arranged, with high positive potential with respect to the cathode. So long as the anode potential is below a certain critical value, the magnetic field prevents all but a small fraction of the electrons from reaching the anode. At the two ends, guard electrodes with potential somewhat below the cathode potential prevent the electrons from escaping. Thus the space accessible

to electrons is limited from all sides. Into this space the cathode will pour electrons until the potential in the axis is depressed to very nearly cathode potential, and equilibrium is established **[Gabor 1947].**

At present there is a significant requirement for the development of devices for focusing high-energy intense ion beams of the solution of actual scientific and technological problems (inertial thermonuclear fusion on heavy and light ions, radiotherapy, high energy investigations, research of radiation resistance of materials, implantation metallurgy, etc.). Last time Gabor lenses with essentially larger focusing force are used. It is essential that the charge of focused beam is compensated in these lenses. With energy and current growth of accelerated beams Gabor lenses should replace the conventional ones. Gabor lens or plasma lens investigation is performed in many scientific centers such as Lawrence Berkeley Laboratory

1.3 Historical Development

In **1947 Gabor** proposed the space charge lens (Gabor lens) for electrostatic focusing of ion beam. Gabor lens cosists of cylindrical column of electron plasma confined with magnetic field. According to **Ivanov [2004],** panofsky and Baker performed experiments on high-energy ion beams focusing by magnetic plasma lens which represents itself the discharge in plasma.

In **1965 Morozov** proposed a plasma electrostatic lens in a which magnetic surfaces are the equipotentials of electric field. According to **Morozov 1965** this direction was successfully developed in experiments of Goncharov, i.e, for ion beam focusing with an energy of tens kV. In

the **Morozov** lens the electric potentials were inserted into plasma by the concentric ring electrodes. In this case, the system of the ((charged)) magnetic surfaces is created in the plasma. It is supposed that in the applied strong magnetic field the transverse current is absent. For the long **Morozov** lens, it is worth-while to place the concentric ring electrodes on the lens faces (or near by them at lateral surface), i.e. at the input and output of the focusing beam.

In eighties for focusing ultra-high energy electron beams it was proposed ((passive)) plasma lenses based on conception of magnetic self-focusing. Later the conception of ((passive)) plasma lenses was expanded on more worth-while adiabatic plasma lenses **[Morozov 1965]**.

In **1999 Goncharov** worked on focusing a heavy-ion beams, high current, and large-area with a plasma lens. Operation of the lens with resistance voltage divider to supply the ring electrode voltages was then not reasonably possible because of high currents involved, and used instead an RC-divider which was able to hold the electrode voltages constant throughout the beam. These experiments carried out at Kiev provided the Berkeley. Some early results of these experiments describing the optimum operating conditions have been briefly summarized previously **[Goncharov, et.al 2000]**.

1.4 Gabor Lens Applications

Gabor or plasma lenses have been used to focus intense beams of positive ions at energies from 10 keV to 5 MeV. Although theoretically, the focusing capability of a Gabor lens looks very promising, relatively little experimental research has been performed to test and develop this device for practical use. A Gabor lens could also be used for negative-beams, e.g., H^-, provided that the electrons are replaced by positrons **[Palkovic 1989].**

Gabor lens (also called space-charge lens) show that this lens is capable of providing much stronger focusing than other lenses. Gabor lenses provide strong symmetric cylinder focusing for low energy ion beams using confined non-neutral plasma. They need reduced magnetic and electrostatic field strength or a reduced installation length to provide a given focal length compared with conventional systems like quadrupole and magnetic solenoids. The density distribution of the enclosed space charge is given by the enclosure conditions in transverse and longitudinal direction. For homogeneous charge density distribution the resulting electrostatic field and the focusing forces inside the space charge cloud are linear. Additionally in case of a positive ion beam the space charge of the confined electrons causes compensation of the ion beam space charge forces. Hence all resolving forces on the beam ions are linear and thus the transformation is linear as well and the aberrations are minimal. Therefore space charge lenses are a serious alternative to inject space charge dominated low energy heavy ion beam into a RFQ **[Meusel,et.al 2001].**

.

1.5 Aim of the Project

It seems that the Gabor lens has escaped its fair share of attention in the literature for there is a little published data on its electron-optical characteristics. Since the main features of a Gabor lens is a combination of an electrostatic lens and a magnetic lens along its main axis, thus the present work would be first performed by proposing simple designs for these two charged-particles lenses. This project aims to study computationally the trajectories of an electron beam traversing the combined electrostatic and magnetic fields and to investigate the optical properties of this lens such as the focal length and spherical and chromatic aberration coefficients. The first order optical properties are computed by solving the trajectory equation of the charged-particles beam traversing both field distributions. Fundamental computations of the electron-optical focal properties are carried out under various operational conditions that are well-known in electron optics. Excitation of the two lenses constituting a Gabor lens has been taken into account in the present investigation.

CHAPTER TWO

THEORETICAL CONSIDERATIONS

2. THEORETICAL CONSIDERATIONS

2.1 Introduction

Electron and ion optics is the theory and practice of production, control, and utilization of charged-particle beams. Charged-particle beams can only be controlled (accelerated, focused, and deflected) by external electromagnetic fields. Electric fields are produced by set of electrodes held at suitably chosen voltage. Coils surrounded by ferromagnetic materials provide a magnetic field. Different symmetries may be utilized for electron and ion optical element such as lenses and deflectors.

In a typical electron-optical device, the electron beam originates with some energy from the source. It enters the focusing field of an objective lens at a certain acceptance angle, to be focused to a point image at a reasonable working distance behind the lens. However, due to the geometrical and chromatic aberrations of the lens, a point image can never be achieved. There will be a crossover of different trajectories instead. This crossover can be imaged by a projector lens and deflected by a suitable deflector element. The deflector itself is a source of additional aberrations **[Maloff** and **Epstein 1938]**.

2.2 Trajectory Equations

When a charged particle travels through a region containing a magnetic field or an electrostatic field, or both, forces will be exerted on it that deflect it and, in the case of electrostatic field, alter its speed. The

path of the incoming accelerated charged-particles beam depends on the properties of the axial field it traverses.

2.2.1 Paraxial-ray equation for an electrostatic field

The trajectory of a beam traversing an electrostatic symmetrical electron or ion optical system is given by **[Hawkes, 1972]:**

$$r'' + r' \cdot \frac{V'}{2V} + \frac{V''}{4V} \cdot r = 0 \quad \ldots\ldots\ldots\ldots\ldots\ldots\ldots\ldots\ldots\ldots\ldots\ldots\ldots\ldots\ldots\ldots (2.1)$$

where *r* is the radial displacement from the optical axis *z*, the primes denote a derivative with respect to *z*. *V= V (z)* is the electrostatic potential distribution along the optical axis *z*. Equation (2-1) is a linear homogeneous second-order differential equation, known as the paraxial-ray equation which describes the paths of charged particles moving through a rotationally symmetrical electrostatic field characterized by the potential function *V*. The paraxial-ray equation was first derived by Busch in 1926. Many important deductions can be made from this equation **[Hamad 2003]**:

(a) The quotient of charge-to-mass (Q/m) does not appear in the equation. Therefore, the trajectory is the same for any charged particle entering the field with the same initial kinetic energy, but arrives to the same focus at different times.

(b) The equation is homogeneous in V. Therefore, an equal increase (or decrease) in the potential V at all the points of field (i.e. multiplying the potential by any constant) does not change the trajectory.

(c) The equation is homogeneous in r and z which indicates that any increase in the dimensions of the whole system produce a corresponding increase in the dimensions of the trajectory, since the equipotentials, though of the same form, are enlarged. If the object is doubled in size, the image will be doubled in size, the ratio between the two remaining constant.

2.2.2 Paraxial-ray equation for a magnetic field

The motion of a charged-particle (an electron in this case) in an axially symmetrical field may be derived starting from many departure points. One can start from a more familiar method of elementary mechanics. The paraxial-ray equation in a magnetic field of axial symmetry is given by **[Hawkes 1982]:**

$$\frac{d^2 r}{dz^2} + \left(\frac{e}{8mV_r} \right) (B_z)^2 r = 0 \quad \text{..... (2.2)}$$

where e and m are the charge and mass of the electron respectively, $B_z = B(z)$ is the axial magnetic flux density, and V_r is the relativistically corrected accelerating voltage which is given by:

$$V_r = V_a\left(1 + 0.978\times10^{-6}V_a\right) \quad \text{..... (2.3)}$$

V_a being the applied accelerating voltage. It can be easily realized from equation (2-2) that the force driving the electrons towards the axis is directly proportional to the radial distance r. This is the principle of a focusing field. Furthermore, this force is proportional to the square of the magnetic flux density which means that if the direction of the magnetic field is reversed by reversing the current, the direction of the force towards the axis should not change, i.e. there will be no change in the focus.

2.2.3 Paraxial-ray equation for combined electrostatic and magnetic fields

For combined electrostatic and magnetic field in the non-relativistic case the trajectory equation is given by **[Myers.l.M 1939]**.

$$r'' = -r' \cdot \frac{V'}{2V} - \frac{V''}{4V} \cdot r - \frac{eB_z^{\,2}}{8mV_a} \cdot r \quad \text{..... (2.4)}$$

The three terms on right-hand-side of equation (2.4) represent focusing processes. The first term arises from acceleration along the axis. The term reduces the envelope angle, r', when particles accelerate. The second term represents electrostatic focusing from radial components of applied electric fields. The effect is important in low-energy electron-optical systems or in acceleration columns. Usually, one may neglect this term when beams have high kinetic energy. The third term describes

magnetic focusing from applied solenoidal fields. Solenoidal lenses are common in electron beam transport systems at low or moderate energies. Solenoidal fields are seldom used for ion transport since they are ineffective for focusing heavy particles because the number of ampere-turns (NI) required to excite the solenoid increases with the increase of the particle's mass**[Myers 1939]**.

2.3 Axial Field Models

It is often desirable to perform a rapid approximate evaluation of lens properties without actually carrying out a detailed analysis. This can be accomplished if one has a simple mathematical model for the lens, i.e. an approximation for the axial field distribution that is reasonably close to the real one and allows a solution in closed form or an approximation in simple terms.

2.3.1 The immersion lens field model

The axial field of an electrostatic immersion lens has two different constant potentials at its sides. This means that the electrostatic field $V'(z)$is zero at the two terminals. Immersion lenses accelerate or retard the particles while the beam is focused. In the present investigation the electrostatic immersion lens and its corresponding axial field distribution have been taken into consideration.

2.3.2 The rectangular magnetic field model

The magnetic rectangular field B_z has a constant maximum value B_m given by **[Hawkes P.W. 1972a]:**

$$B_z = B_m \qquad -L/2 \le z \le L/2 \ldots\ldots\ldots\ldots\ldots\ldots\ldots\ldots\ldots\ldots\ldots\ldots \quad (2.5)$$

and

$$B_z = \mu_0 NI / L \ldots\ldots\ldots\ldots\ldots\ldots\ldots\ldots\ldots\ldots\ldots\ldots\ldots\ldots\ldots\ldots\ldots \quad (2.6)$$

where *NI* is the number of turns of the current-carrying circular coil, *I* is the energizing d.c. current in the coil, and ($\mu_0 = 4\pi * 10^{-7} \mathrm{H}.m^{-1}$) is the permeability of free space. Figure (2.1) shows the rectangular magnetic flux field B_z.

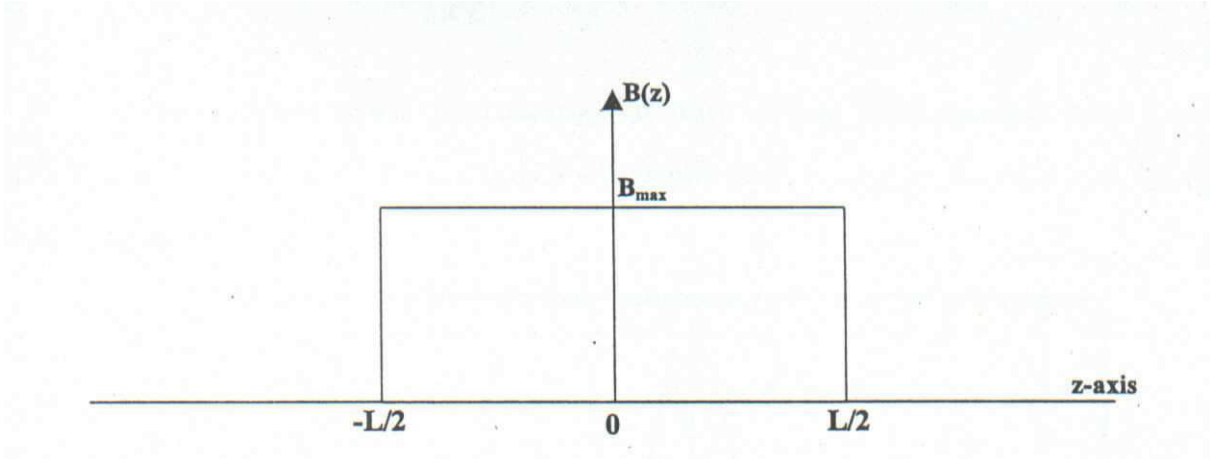

Figure 2.1. The axial flux density distribution in rectangular field model.

Figure (2.2) shows the designed electrostatic and magnetic lens (Gabor lens) with its geometrical parameter, such as the lens length L, separation distance between the two electrodes **s**, and the immersion lens radius R.

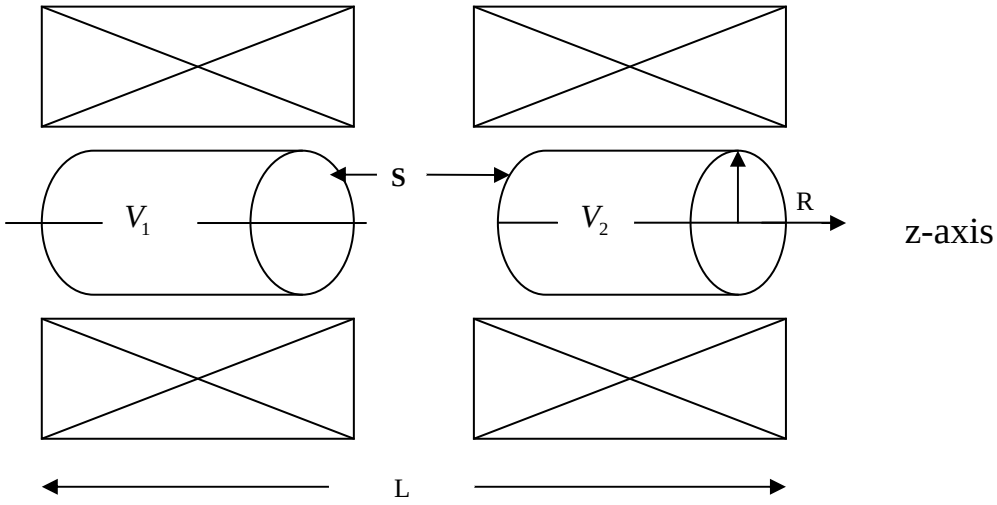

Figure 2.2. The proposed design of Gabor lens

2.4 Lens Aberrations

The quality of any charged-particle optical system depends not only upon the energy of the charged particle but also upon the aberrations. The electron paths, which leave points of the object close to the axis at small inclinations with respect to the axis, intersect the image plane in points forming a geometrically similar pattern. This ideal image is known as the Gaussian image, and the plane in which it is formed as the Gaussian image plane. If an electron path leaving an object point a finite distance from the axis with a particular direction and velocity intersects the *Gaussion image plane* at a point displaced from the

Gaussian image point, this displacement is defined as *aberration***[**see for example**, El-Kareh** and **El-Kareh 1970, Hawkes 1972].**

The aberrations can arise for a number of reasons. However, the two most important aberrations in an electron-optical system are spherical and chromatic aberration. Thus in the present work particular attention was paid to the computation of these two aberrations in a Gabor lens, since unfortunately they received only limited attention in the published investigations by such lens users **[Klemperer 1971].**

Spherical aberration is one of the most effective geometrical aberrations and can be defined in both light optics and electron optics, as the change in focal properties of a lens with the height of the ray from optical axis. Off-axis charged-particles spend less time in the field than do paraxial charged-particles because they do not penetrate as far into the field, and as a result the focal distance is longer for charged-particles whose trajectories make larger angles with the axis than for paraxial charged-particles **[Rempfer 1990].**

Chromatic aberration in light optics refers to the change in focal properties with the wavelength of light. In electron optics it refers to the change in focal properties with kinetic energy of the charged-particles; lower-energy charged-particles penetrate less far into the field than do higher-energy charged-particles, and therefore spend less time in the field and are less strongly converged by the field. Consequently the focal distance is longer for low-energy charged-particles than for high-energy charged-particles [**Rempfer 1990, Rempfer** and **Griffith 1992].**

The spherical and chromatic aberration coefficients are denoted by C_s and C_c respectively. In the present investigation the values of C_s and C_c have been computed for images formed by the combined electrostatic and magnetic lenses and normalized in terms of the image side focal length, i.e. the relative values of C_{si}/f_i and C_{ci}/f_i are investigated as figures of merit which are dimensionless. The spherical aberration coefficient C_s and the chromatic aberration coefficient C_c referred to the image side are calculated from the following formulas [**Szilagyi et al 1987]:**

$$C_{si} = \frac{V^{\frac{-1}{2}}(z_i)}{16 \cdot r_i'^4} \int_{z_0}^{z_i} \left[\frac{r^4}{V^2(z)} \right] \left\{ \begin{array}{l} \frac{5 \cdot V''^2(z)}{4} + \frac{5 \cdot V'^4(z)}{24 \cdot V(z)^2} + \frac{14 \cdot V'^3(z) \cdot r'}{3 \cdot V(z) \cdot r} - \\ \frac{3 \cdot V'^2(z) \cdot r'^2}{2 \cdot r^2} - \frac{e \cdot V(z) \cdot B'^2(z)}{m} + \frac{3 \cdot e^2 \cdot B^4(z)}{8 \cdot m^2} + \\ \frac{e \cdot V(z) \cdot B^2(z) \cdot r'^2}{m \cdot r^2} + \frac{3 \cdot e \cdot B(z) \cdot B'(z) \cdot V'(z)}{m} - \\ \frac{35 \cdot e \cdot B^2(z) \cdot V'^2(z)}{16 \cdot m \cdot V(z)} + \frac{2 \cdot e \cdot B^2(z) \cdot V'(z) \cdot r'}{m \cdot r} \end{array} \right\} dz \quad ..(2.7)$$

$$C_{ci} = \left(\frac{V^{\frac{1}{2}}(z_i)}{r_i^{'2}} \right) \int_{z_0}^{z_i} \left\{ \left[\frac{V''(z)}{4 \cdot V(z)} - \frac{e \cdot B^2(z)}{8 \cdot m \cdot V(z)} \right] \cdot r^2 + \frac{V'(z) \cdot r' \cdot r}{2 \cdot V(z)} \right\} \frac{dz}{(V(z))^{\frac{1}{2}}} \quad \text{.....(2.8)}$$

where $V_i = V(z_i)$ is the axial potential at the image where $z = z_i$. The integrations given in the above equations are executed by means of Simpson's rule. It should be noted that C_s and C_c in the object plane can be expressed in a similar form of equations (2.7) and (2.8) where $V_i^{\frac{1}{2}}$ and r_i' are replaced by $V_o^{\frac{1}{2}}$ and r_o' respectively. More details concerning spherical and chromatic aberrations in electron-optical instruments are found in many publications **[**see for example, **Hawkes 1972, Hawkes** and **Kasper 1989].**

2.5 Definitions and Operating Conditions

Some definitions and operating conditions of charged-particle optical system are given in this section.

Object side: The side of lens at which the charged particles enter.

Image side: The side of lens at which the charged particles leave.

The object plane (z_0): The plane at which the physical object is placed as shown in figure (2.3).

The image plane (z_i): The plane at which the real image of the object plane z_0 is formed on the image side as shown in figure (2.3).

Focal point (f_i): A focal point is the image of a bundle of ray's incident on a lens parallel to the axis. If these rays arrive at the lens from the object side, then these rays are collected at the image focal point f_i.

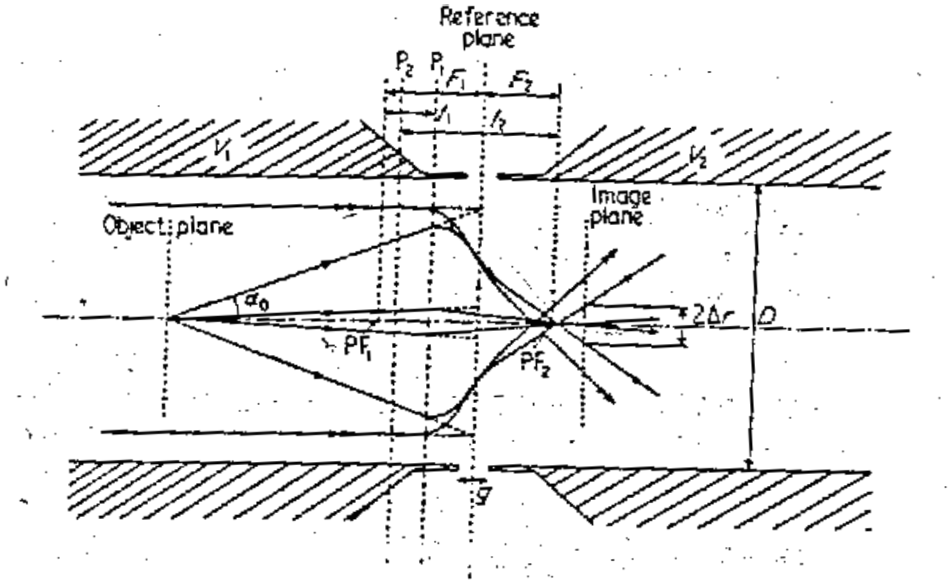

Figure 2.3. The cardinal elements of an axially symmetric lens.

Magnification (*M*): In any optical system the ratio between the transverse dimension of the final image and the corresponding dimension of the original object is called the lateral magnification:

$$M = \frac{(image \cdot height)}{(object \cdot height)}$$

There are three magnification conditions in which a lens or deflector can operate, namely **[Munro 1975]:**

a) **Zero magnification condition:** In this case of operating condition $z_o = -\infty$ as shown in figure 2.4. The final probe-forming lens in a scanning electron microscope (SEM) is usually operated in this condition.

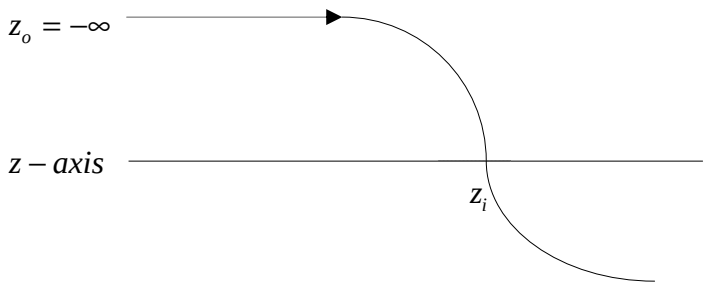

Figure 2.4. Zero magnification condition

b) **Infinite magnification condition:** The operating condition is such that $z_i = +\infty$ as shown in figure 2.5. The objective lens in a transmission electron microscope (TEM) is usually operated in this condition.

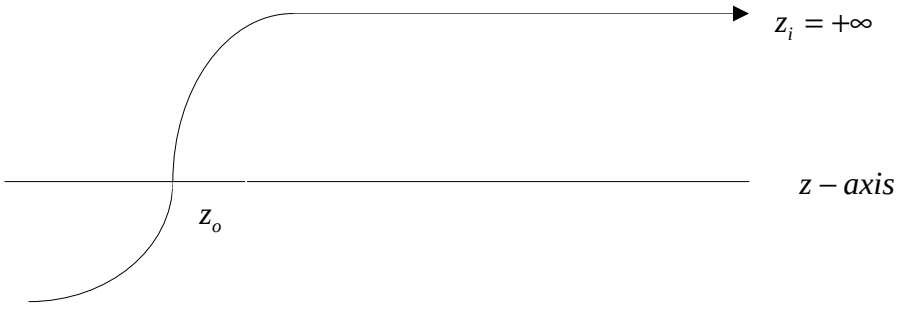

Figure 2.5. Infinite magnification condition

c) **Finite magnification condition:** the operating condition in this case is that z_0 and z_i are at finite distance, as shown if figure 2.6. The electrostatic lens in field-emission gun is usually operated in this condition.

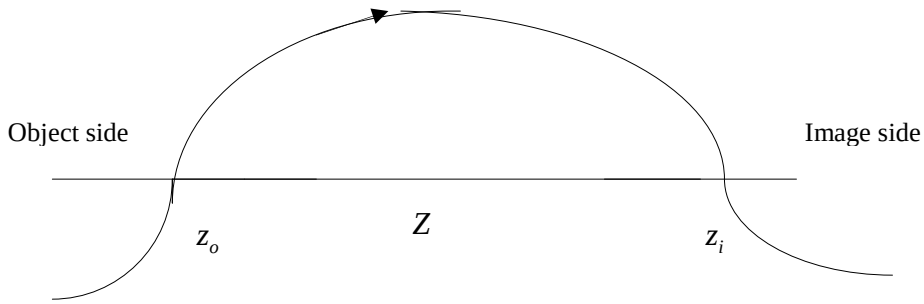

figure 2.6. Finite magnification condition

2.6 Computer program for computing the beam trajectory and optical properties.

A computer program with MathCAD Professional 2001, has been used for determining the trajectory of the electron with the aid of the Runge-Kutta method . By solving the paraxial ray equation of Gabor lens the trajectory and its first and second derivatives can be achieved, then the optical focal properties such as focal length can be computed. The spherical aberration coefficient C_s and chromatic aberration coefficient C_c are computed by using the aberration integral formula given in equation (2.7), (2.8). Figure 2.5 illustrates a block diagram of this computer program.

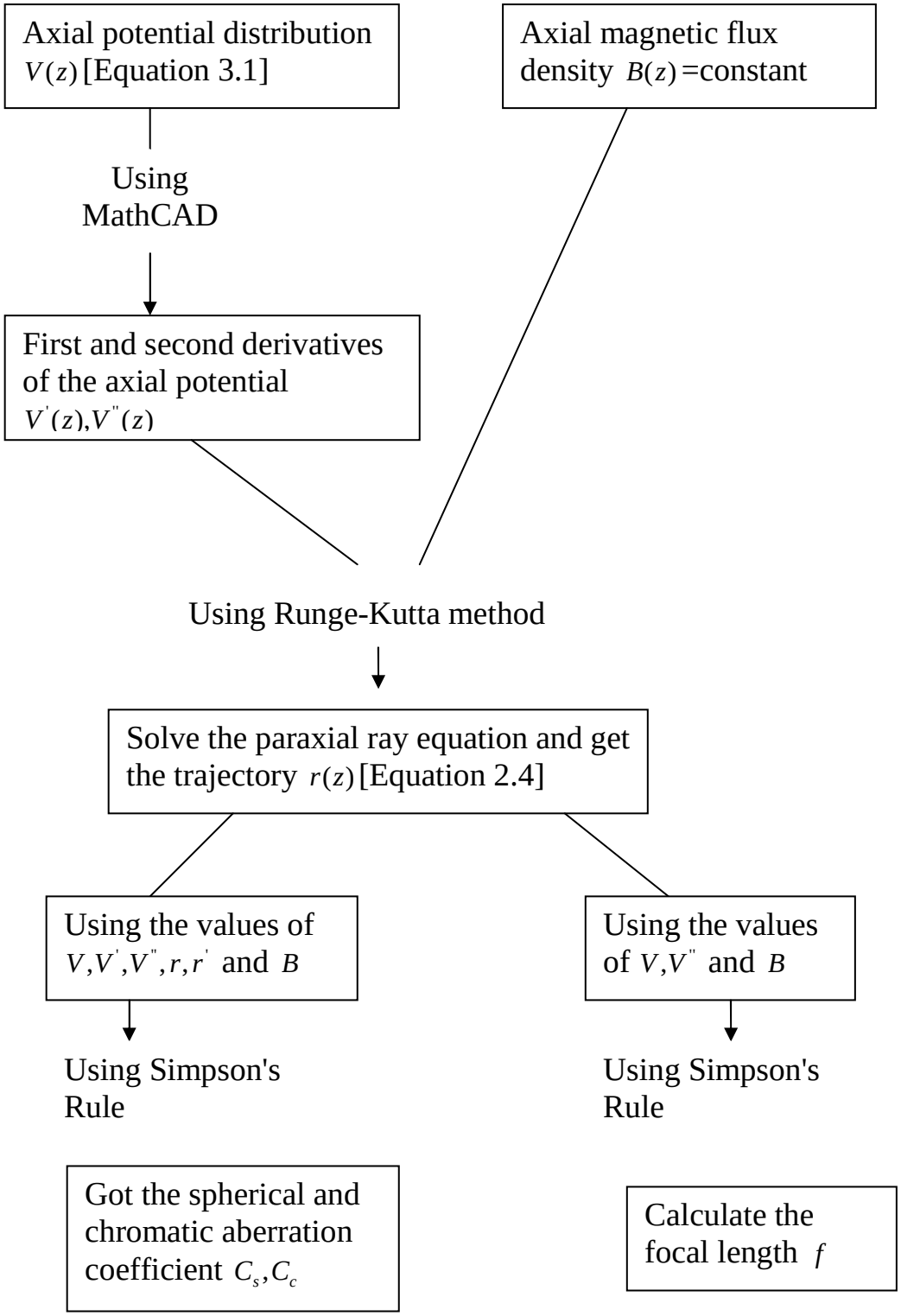

Figure (2.5) A block diagram of the MathCAD program for computing, the axial electric and magnetic flux distributions, the trajectory and the optical properties of Gabor lens.

3. RESULTS AND DISCUSSION

3.1. The Behaviour of the Axial Electrostatic Potential Distribution of an Immersion Lens at Different Separation Distances

The axial electrostatic potential distribution of the immersion lens used in the present work is given by**[Myers. 1939]**:

$$V(z) = V_0 + \frac{\Delta V}{2} + \frac{\Delta V}{b} \cdot \int_0^z e^{\frac{-\pi \cdot z^2}{b^2}} dz \quad \text{..... ....} \quad (3.1)$$

where $V(z)$ is the axial electrostatic potential distribution along the optical axis z, $V_o, \Delta V$ and b are given as below respectively:

$$V_0 = \frac{V_1 + V_2}{2}$$

$$\Delta V = V_2 - V_1$$

$$b = 2 \cdot R \left\{ 0.73 + 0.53 \cdot \left(\frac{s}{2 \cdot R} \right)^2 \right\} \quad \text{.....} \quad (3.2)$$

where R (= 4 cm) is the radius of the electrodes and **s** is the separation distance between the two electrodes (see figure 2.2). Equation (3.1), gives the potential along the optical axis in terms of the potential of the first and second electrodes V_1 and V_2 respectively, the difference of potential of the two electrodes and a variable parameter b which depends on the geometrical

disposition of the two electrodes. It was found that the variation of the parameter b for various sizes and separations of the electrodes was adequately expressed in equation (3.2).

Figure (3.1) shows the axial potential distribution *V*(z) based on the expression given in equation (3.1). The axial potential field have two different constant values at the lens terminals. The voltage applied on the electrode positioned at the right-hand side of the lens is higher than the electrode on the left-hand side (accelerating lens). Constant potential field means zero electric field since $V' = \frac{dV}{dz}$, and this is appears clearly in figure (3.2), where the electric field is zero at the lens terminals. Therefore, the charged-particles move in straight line outside the lens, since there is no force affect the charged-particle beams.

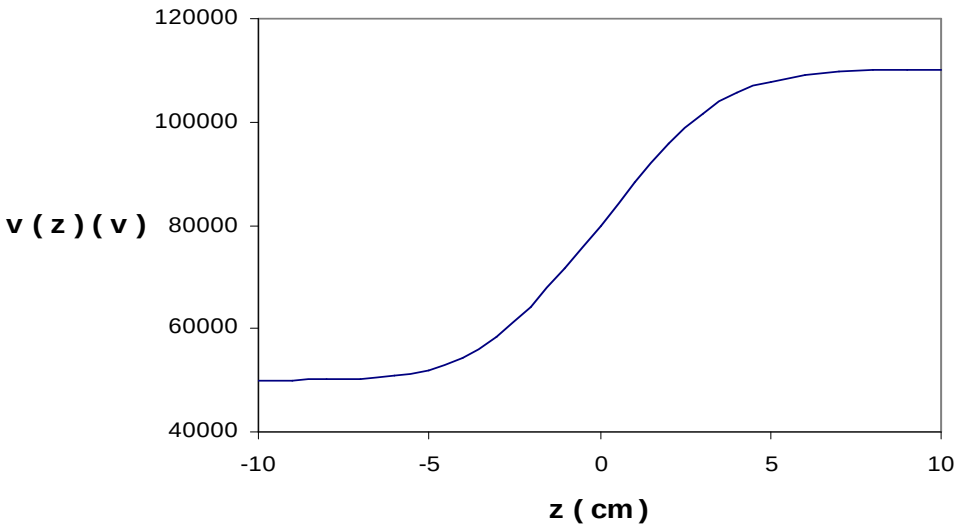

Figure 3.1. The axial electrostatic potential field distribution of the two electrodes immersion lens when V_1 *= 50 kV,* V_2 *= 110 kV,s = 2 cm and R = 4 cm*

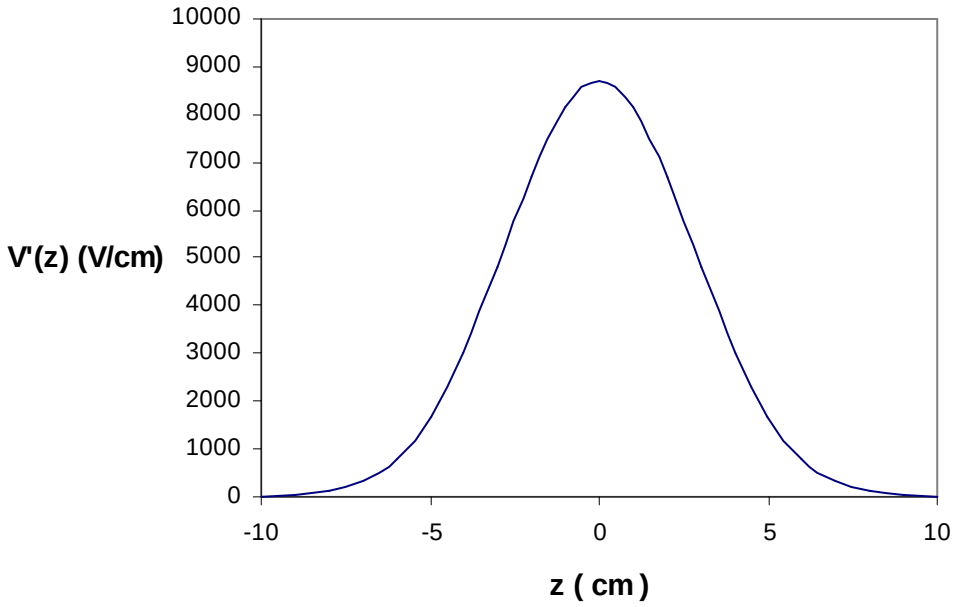

Figure 3.2. The first derivative V' (z) of the two electrodes immersion lens when V_1 = 50 kV, V_2 = 110 kV, s = 2 cm and R = 4 cm.

The axial potential distributions at three values of the separation distance **s** are shown in figure (3.3). These potentials are similar in their general form. All curves intersect at a common point situated at the center of the separation irrespective of the relative separation distance **s**. The potential V (z) at this common point of intersection (z=0) equals to 80kV, which is the average of the potentials applied on the two electrodes. This result is valid at all values of the applied voltage. Furthermore, this common point can be used as a criterion for the classification of the lens whether it is symmetrical or asymmetrical. The potential on the side of the lower voltage electrode penetrates the hollow cylindrical electrode and its gradient diminishes at a common point (z = -10 cm) irrespective the separation distance **s**. The value of the potential at this point is equal to the voltage applied on the corresponding electrode (i.e. $V(z)$ = 50 kV). On the other hand, the potential

on the side of the higher voltage electrode penetrates the hollow cylindrical electrode region and its gradient diminishes at common point (z = 10 cm) where its value equals to that of the applied voltage (i.e. $V(z)$ = 110 kV).

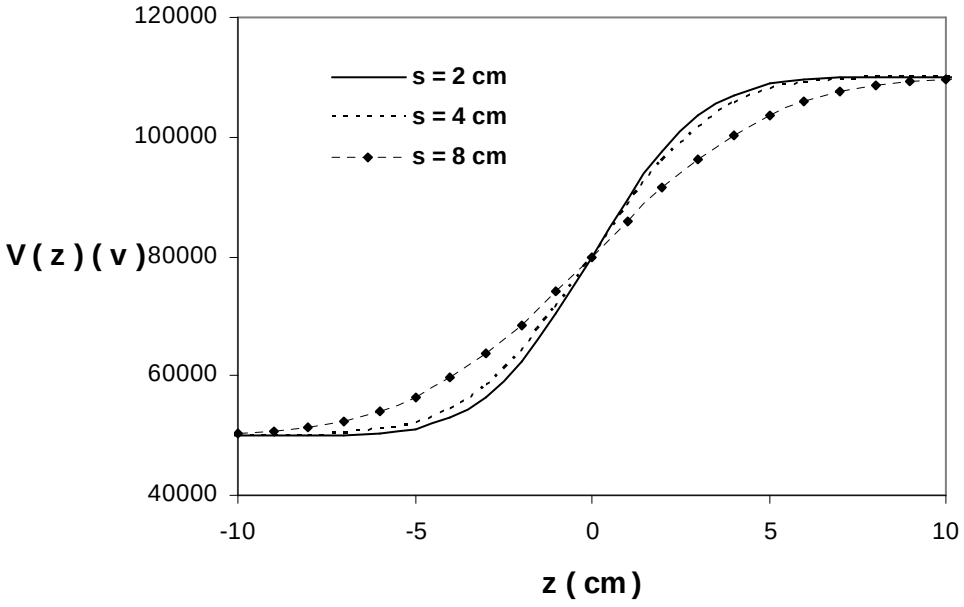

Figure 3.3. The axial potential distribution of the two electrodes immersion lens at various values of the separation distance ***s****.*

3.2. Electron Beam Trajectory Under Zero Magnification Condition

The electron beam path along the electrostatic and magnetic fields under zero magnification condition and accelerating mode of operation has been considered.

Figure (3.4) shows the trajectories of an electron beam traversing Gabor lens field at various values of both voltage ratio $\frac{V_2}{V_1}$ and separation distance **s,** at constant values of both current-turn NI = 1250 (A-t) and lens

length L = 20 cm . These trajectories have been computed with the aid of the paraxial ray equation (2.4) of the combined electrostatic and magnetic lens and the axial potential field distribution $V(z)$ given in equation (3.1). The trajectories are similar in their general form. The effect of the separation distance **s** is seen clearly on the trajectories that intersects the optical axis. The gradient of the beam trajectory decreases with increasing the separation distance **s** when the voltage ratio $\frac{V_2}{V_1} = 22$, the radial displacement of the electron beams r = - 0.58 cm when the separation distance **s** =2 cm, while when **s** = 5 and 8 cm the radial displacement r = -0.4 cm and -0.22 cm respectively. This is due to the fact that the electron beam travel in the gap region between the two electrodes where the effect of the electrode potential is less in this region on the electron beam. Furthermore, the trajectories of the beam at the exit side increases with increasing voltage ratio irrespective of the separation distance **s**. The beam is in the state of convergence at all points on the image side beyond the center of the separation.

Figure (3.5) shows the trajectories of an electron beam traversing Gabor lens field at various values of both current-turn NI and lens length L, and at constant values of both voltage ratio $\frac{V_2}{V_1}$=8 and separation distance **s**= 8 cm . These trajectories have been computed with the aid of the paraxial ray equation (2.4) of the combined magnetic and electrostatic lens. The effect of the lens length L is seen clearly on the trajectories that intersect the optical axis. The gradient of the beam trajectory decreases with increasing the lens length L. Furthermore, the gradient of the beam trajectories at the image side increases with increasing current-turn NI irrespective of the lens length L. The beam is in the state of convergence at all points on the image side beyond the center of the length.

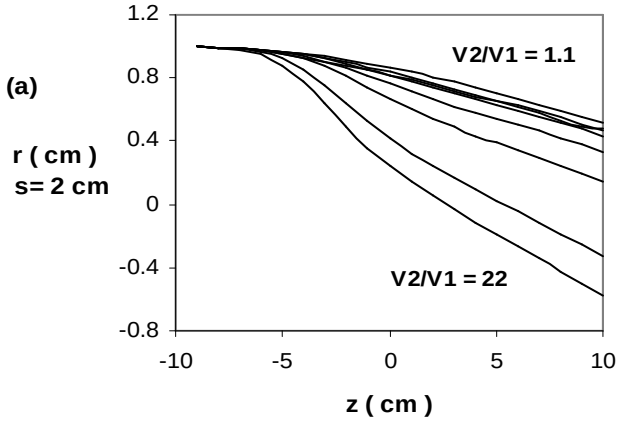

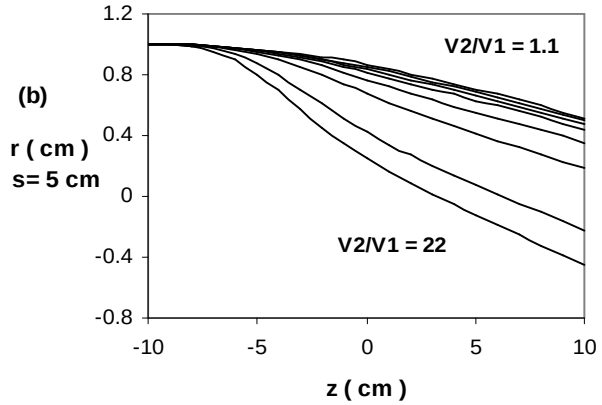

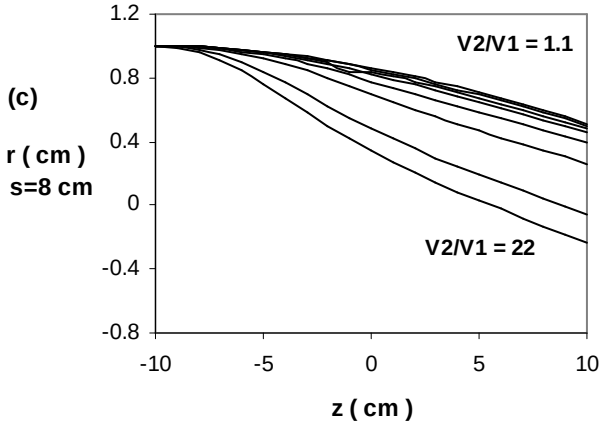

Figure 3.4. The electron beam trajectories in Gabor lens under zero magnification condition at various values of separation distance s and voltage ratio $\frac{V_2}{V_1}$*, and at constant current-turn NI = 1250 (A-t) and lens length L = 20 cm.*

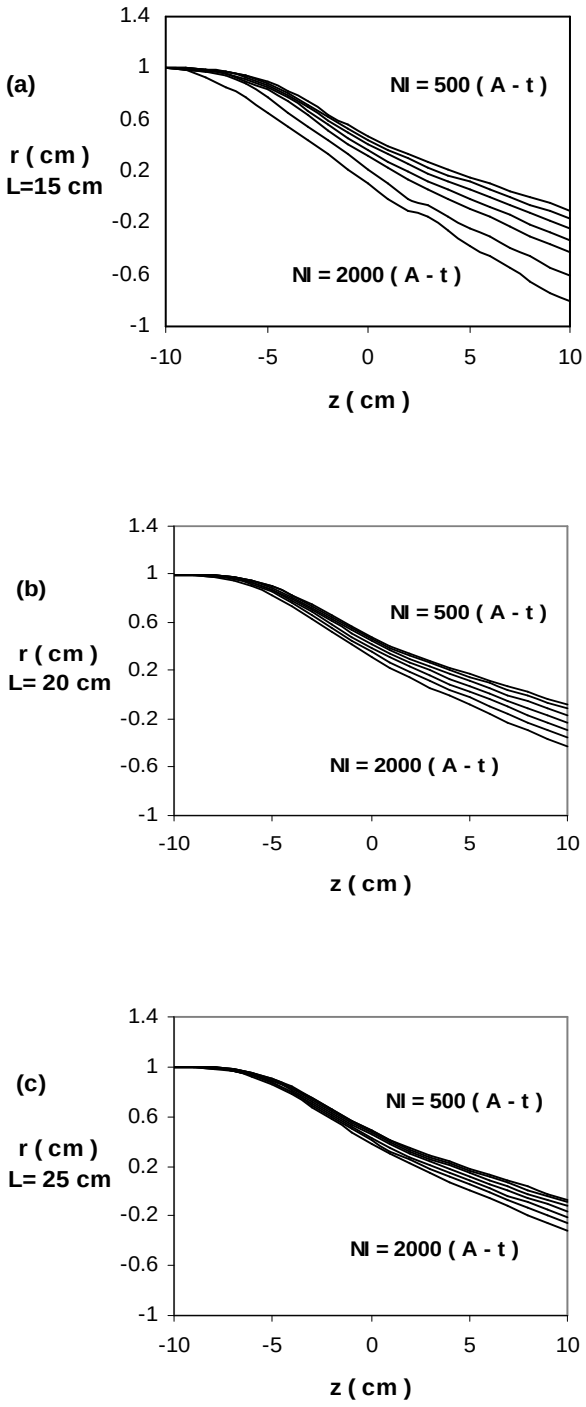

Figure 3.5. The electron beam trajectories in Gabor lens under zero magnification condition at various values of lens length L, and current-turn NI and at constant voltage ratio $\frac{V_2}{V_1}$ *= 8 and separation distance s =8 cm.*

3.3. Relative Aberration Coefficients Under Zero Magnification Condition

The spherical and chromatic aberration coefficients have been given considerable attention in the present work since they are the two most important aberrations in electron optical systems. The present investigation has been focused on their effect on the image side and has been normalized in terms of the image side focal length, i.e. the relatives values of $\frac{C_{si}}{f_i}$ and $\frac{C_{ci}}{f_i}$ are investigated as figures of merit which are dimensionless.

3.3.1 Image-side relative spherical aberration coefficient

The relative spherical aberration coefficient $\frac{C_{si}}{f_i}$ in the image-side of the Gabor lens as a function of the voltage ratio at various values of the separation distance **s** and at constant values of both the current- turn NI=1250(A-t) and lens length L=20cm when the lens operated in accelerating mode and under zero magnification condition is shown in figure (3.6). The trajectories shown in figure (3.4) with the aid of equation (2.4) have been used for computing the image-side relative spherical aberration coefficients. The image-side relative spherical aberration coefficients have minima values as shown in Table (3.1). The minimum value of $\frac{C_{si}}{f_i}$ decreases with increasing the separation distance **s**. One can notice from Table (3.1) that there is no need to increase the voltage ratio since the values of the relative aberration coefficients are small and from the electron-optical point of view all these values are acceptable. It is possible to decrease the separation distance between the electrodes to obtain the low value for the relative spherical aberration coefficient, but one should be

careful since any reduction in the lens axial length is, of course, limited by the voltage ratio at which no electrical breakdown would occur. Under normal operational vacuum pressure in electron microscopy the limiting electric field at which breakdown would occur is about 15 kV/mm. This is due to the fact that the sparking potential decreases with the increase of the product (p**s**) of gas pressure p and gap length **s;** this relation is known as Paschen's law **[Kuffel** and **Abdullah 1979].**

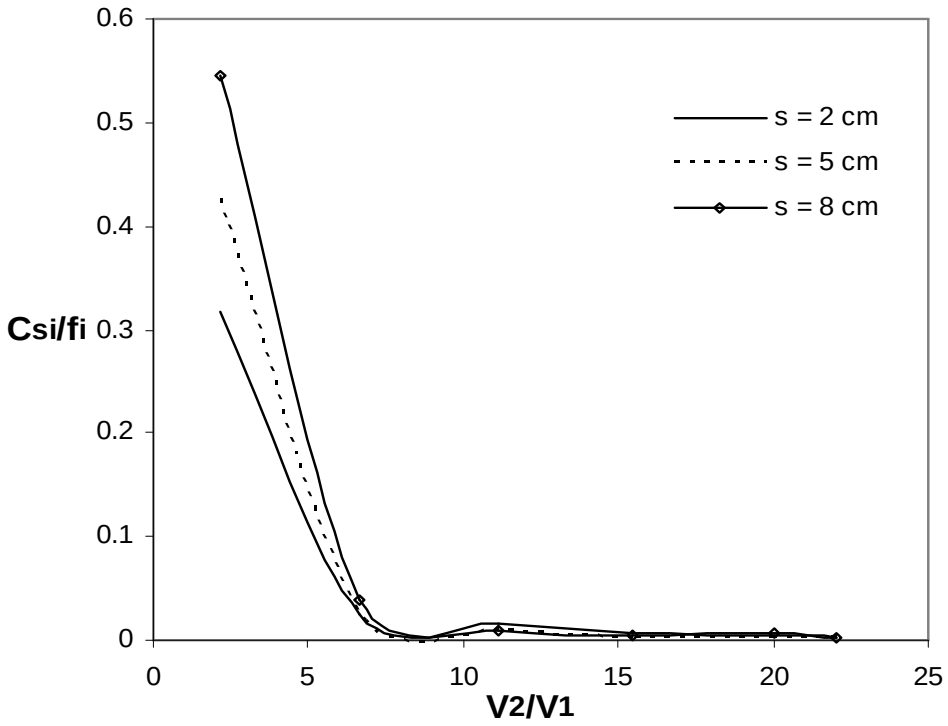

Figure 3.6. The image-side relative spherical aberration coefficient $\frac{C_{si}}{f_i}$ *as a function of the voltage ratio* $\frac{V_2}{V_1}$ *at various values of the separation distance* ***s*** *and at constant current-turn NI = 1250 (A-t) and lens length L = 20 cm.*

Table (3.1). The minimum value of the image-side relative spherical aberration coefficient and corresponding focal length for different values of both the separation distance **s** *and voltage ratio* $\frac{V_2}{V_1}$ *(NI = 1250 A-t, L = 20 cm)*

s (cm)	$\left(\frac{C_{si}}{f_i}\right)_{\min}$	f_i (cm)	$\frac{V_2}{V_1}$
2	.015	21.2	8
5	.011	22.37	7
8	.0085	23.85	7

Figure (3.7) shows the image-side relative spherical aberration coefficient $\frac{C_{si}}{f_i}$ of the Gabor lens as a function of the number of the current-turn at various values of the lens length L and at constant values of both the voltage ratio $\frac{V_2}{V_1}$ = 8 and separation distance **s** = 8 cm under zero magnification condition with the aid of the trajectories shown in figure (3.5) and equation (2.4). In general the values of $\frac{C_{si}}{f_i}$ are electron-optically acceptable since they are less than one, even for high value of the current-turn NI the relative spherical aberration coefficient increases but still have acceptable values.

Although the minimum value of $\frac{C_{si}}{f_i}$ decreases with increasing L as shown in Table (3.2), but the decrement is small in comparison with the increase in the current-turn, which it is not preferable. Therefore, one can chose the suitable value of the lens length L with small value for the current-turn NI.

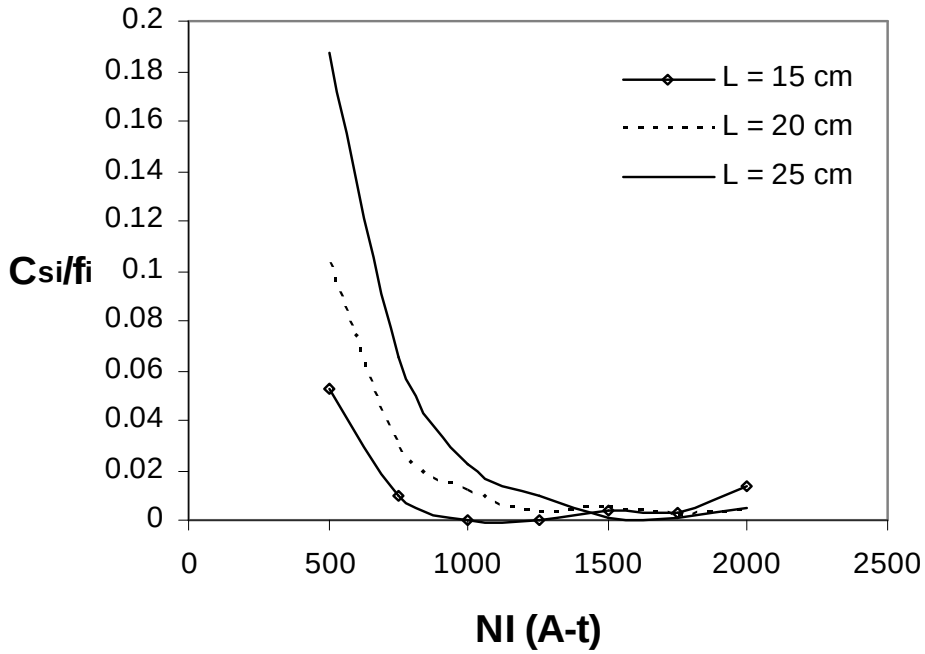

Figure 3.7. The image-side relative spherical aberration coefficient $\frac{C_{si}}{f_i}$ *as a function of the current-turn NI at various values of lens length L and at constant voltage ratio* $\frac{V_2}{V_1}$ *= 8 and separation distance* ***s*** *= 8 cm.*

*Table (3.2). The minimum value of the image-side relative spherical aberration coefficient and the corresponding focal length for different values of both lens length L, and current-turn NI (****s*** *= 8 cm ,* $\frac{V_2}{V_1} = 8$ *)*

L (cm)	$\left(\frac{C_{si}}{f_i}\right)_{\min}$	f_i (cm)	NI(A-t)
15	.004	22	1000
20	.0031	23.9	1250
25	.00078	25	1500

3.3.2 Image-side relative chromatic aberration coefficient

The voltage of the trajectories shown in figure (3.4) and equation (2.4) have been used for computing the image-side relative chromatic aberration coefficient $\frac{C_{ci}}{f_i}$ as a function of voltage ratio $\frac{V_2}{V_1}$ at various values of the separation distance **s** and constant values of NI and L. Figure (3.8) shows that $\frac{C_{Ci}}{f_i}$ increases with increasing $\frac{V_2}{V_1}$ irrespective of the value of **s**. In general the value of $\frac{C_{ci}}{f_i}$ is greater that $\frac{C_{si}}{f_i}$ for the same value of the voltage ratio $\frac{V_2}{V_1}$.

The relative chromatic aberration coefficient $\frac{C_{ci}}{f_i}$ have minima values as shown in Table (3.3). The Table shows that when **s** = 2 cm $\frac{C_{ci}}{f_i}$ has a minimum value at voltage ratio $\frac{V_2}{V_1}$ = 3.66, which is the same value for the minimam relative spherical aberration coefficient (see Table 3.1).

The relative chromatic aberration coefficient referred to the image-side when the lens operated under zero magnification condition has been investigated as a function of current-turn NI, for different values of the lens length L, and at constant values of both the voltage ratio $\frac{V_2}{V_1}$ = 8 and separation distance **s** = 8 cm as shown in figure (3.9). The relative chromatic aberration coefficient $\frac{C_{ci}}{f_i}$ increases with increasing NI irrespective of L.

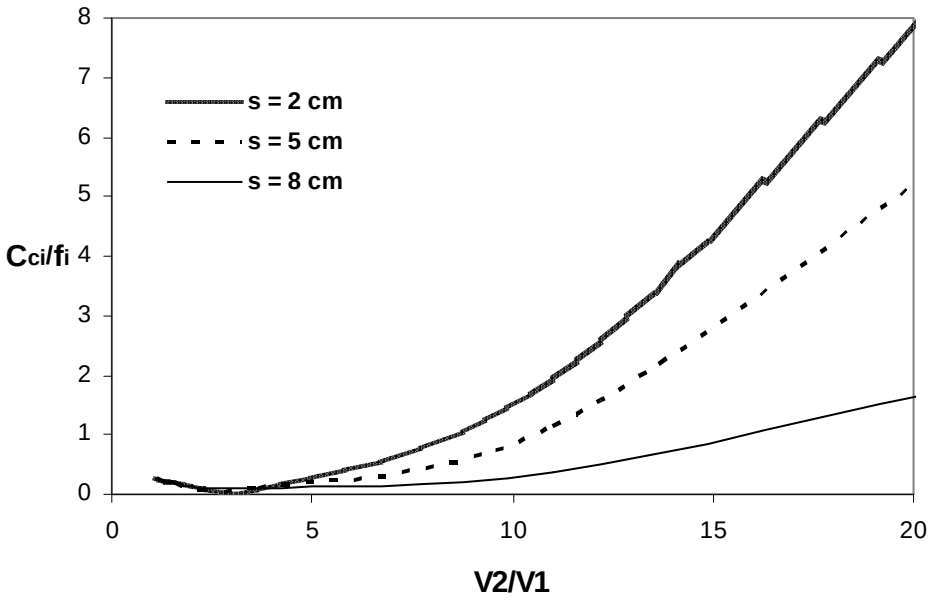

Figure 3.8. The image-side relative chromatic aberration coefficient $\frac{C_{ci}}{f_i}$ *as a function of the voltage ratio* $\frac{V_2}{V_1}$ *at various values of the separation distance* ***s*** *and at constant current-turn NI = 1250 (A-t) and lens length L = 20 cm.*

Table (3.3). The minimum value of the image-side relative chromatic aberration coefficient and the corresponding voltage ratio $\frac{V_2}{V_1}$ *for different values of the separation distance* ***s*** *(NI = 1250 A-t, L = 20 cm).*

s (cm)	$\left(\frac{C_{ci}}{f_i}\right)_{\min}$	$\frac{V_2}{V_1}$
2	.063	3.66
5	.06	2.2
8	.09	2.2

From the figure (3.9) the relative chromatic aberration coefficient has minima values as shown in Table (3.4). The minima values increases with increasing the lens length. The increase of $\frac{C_{ci}}{f_i}$ is very small in comparison with increase in the current-turn NI. Therefore, it is preferable to chose low value for the current-turn NI with electron-optically acceptable value for $\frac{C_{ci}}{f_i}$.

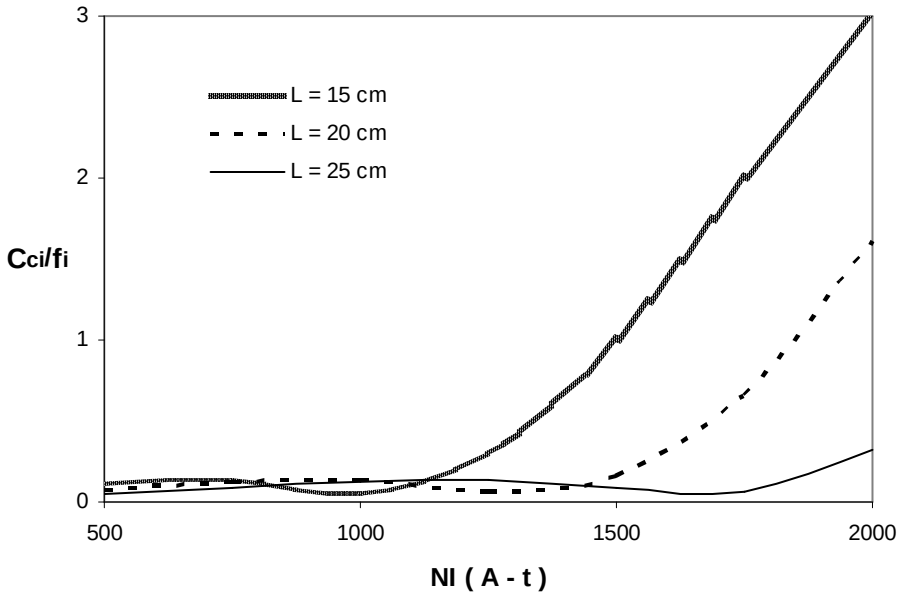

Figure 3.9. The relative image-side chromatic aberration coefficient $\frac{C_{ci}}{f_i}$ *as a function of the current-turn NI, at various values of lens length L and constat value of the voltage ratio* $\frac{V_2}{V_1}$ *= 8 and separation distance* ***s*** *= 8 cm.*

*Table (3.4). The minimum value of the image-side relative chromatic aberration coefficient and the corresponding current-turn NI for different values of the lens length L ($\frac{V_2}{V_1}$ = 8, **s** = 8 cm).*

L (cm)	$\left(\frac{C_{ci}}{f_i}\right)_{\min}$	NI (A-t)
15	0.046	1000
20	0.062	1250
25	0.066	1750

3.3.3 Image-side focal length

The image-side focal length of an electrostatic and magnetic lens can be determined from the following equation **[Myers.l.M 1939]**:

$$f_i = \frac{-1}{r'(z_i)} \quad \text{.....} \quad (3.3)$$

where $r'(z_i)$ is the first derivative of the radial displacement at the image-side. Under zero magnification condition, the image-side focal length f_i of Gabor lens are studied as a function of the voltage ratio $\frac{V_2}{V_1}$ as shown in figure (3.10) for different values of the separation distance **s**, and at constant values of the both current-turn NI = 1250 (A-t) and lens length L = 20 cm. Figure (3.10) shows that f_i decreases with increasing voltage ratio $\frac{V_2}{V_1}$ and increases with increasing the separation distance **s**.

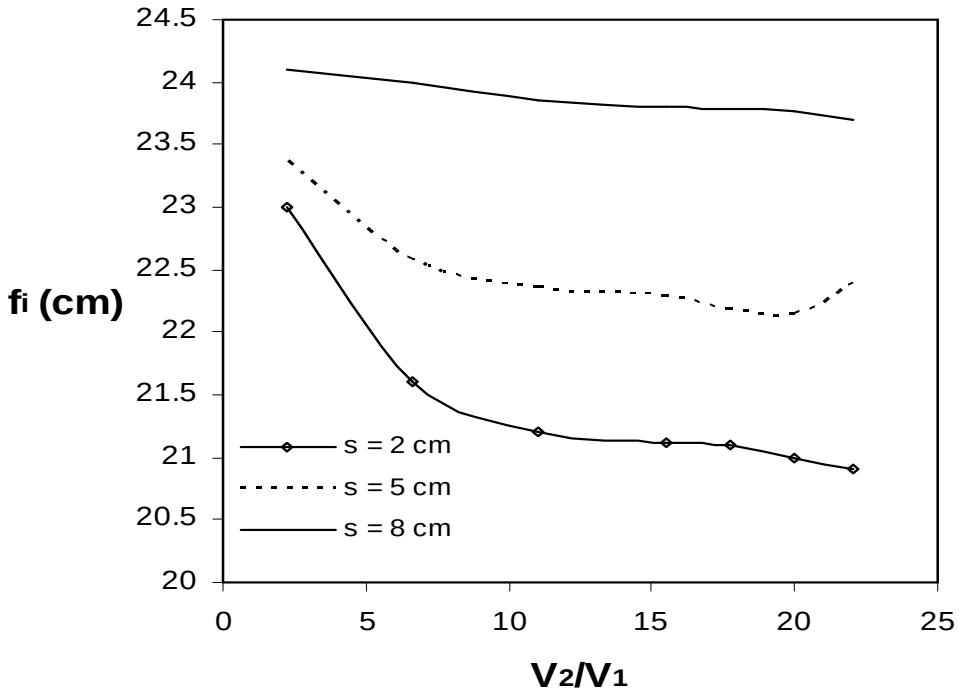

Figure 3.10. The image-side focal length as a function of the voltage ratio $\frac{V_2}{V_1}$ *at various values of the separation distance* ***s*** *and at constant value of both current-turn NI = 1250 (A-t) and lens length L = 20 cm.*

Figure (3.11) shows that the variation of the image-side focal length f_i as a function of NI at various values of the lens length L and at constant values of both the voltage ratio $\frac{V_2}{V_1}$ = 8 and separation distance **s** = 8 cm. It is seen that f_i decreases with increasing NI, this is due to the increase of the lens refractive power with increasing magnetic field. Figure (3.11) shows also that the image-side focal length f_i increases with increasing the lens length L.

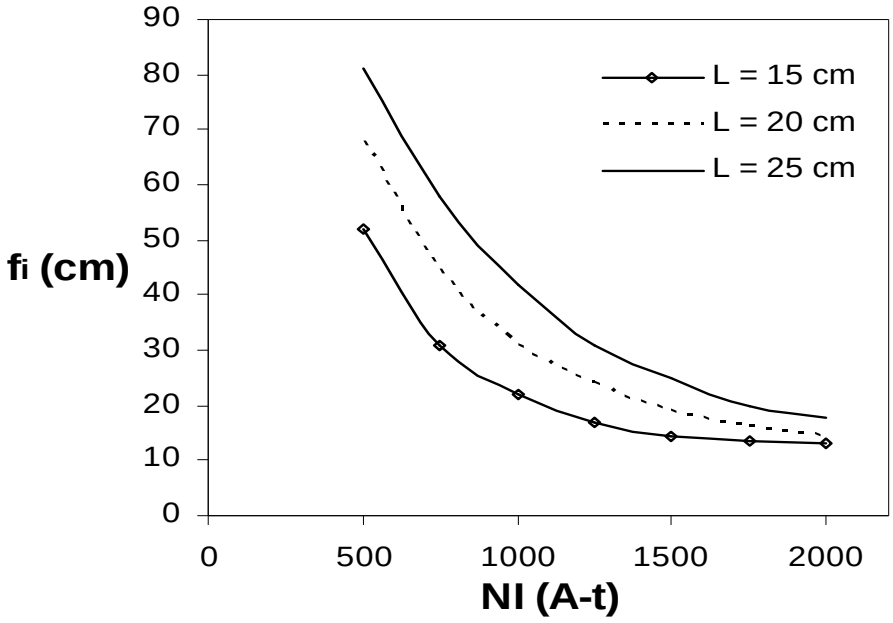

Figure 3.11. The image-side focal length as a function of the current-turn NI at various values of the lens length L and at constant values of both the voltage ratio $\frac{V_2}{V_1} = 8$ *and separation distance s = 8 cm.*

3.4 Electron Beam Trajectory Under Infinite Magnification Condition

The electron beam path along Gabor lens fields under infinite magnification condition has been considered. Figure (3.12) shows the trajectories of an electron beam traversing Gabor lens field operated under infinte magnification condition at various values of both voltage ratio $\frac{V_2}{V_1}$ and separation distance **s** and at constant values of both the current-turn NI = 1250 (A-t) and lens length L = 20 cm. These trajectories have been computed with the aid of the paraxial ray equation (2.4) of the combined electrostatic and magnetic lens and the axial potential field distribution $V(z)$ given in equation (3.1). Figure (3.12) shows that as **s** increases the gradient of the radial displacement of the beam decreases.

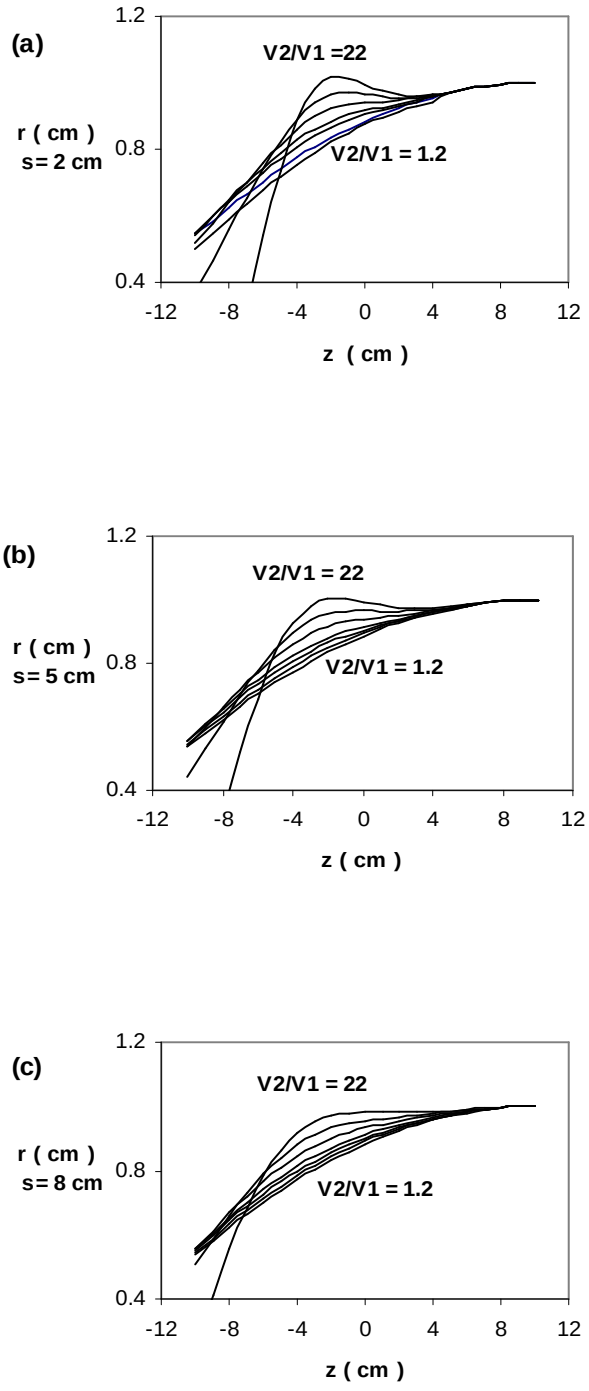

Figure 3.12. The electron beam trajectory in Gabor lens operated under infinite magnification condition at various values of separation distance ***s*** *and voltage ratio* $\frac{V_2}{V_1}$ *and at constant current-turn NI = 1250(A-t) and lens length L=20 cm*

Figure (3.13) shows the trajectories of the electron beam traversing Gabor lens field operated under infinite magnification condition at various values of both current-turn NI and diagonal length L, and at constant values of both voltage ratio $\frac{V_2}{V_1}$ = 8 and separation distance **s** = 8 cm. Figure (3.13) shows that as L increases the gradient of the radial displacement *r* of the beam decreases. Each trajectory represents a lens of specific current-turn NI. The gradient of the radial displacement increases with increasing the current-turn NI.

3.5 Relative Aberration Coefficients of Gabor Lens when Operated under Infinite Magnification Condition

The aberration coefficients of each lens have been computed with the aid of the corresponding trajectory of the electron beam shown in figure (3.12) and (3.13) and equation (2.4). The spherical and chromatic aberration coefficients C_s and C_c respectively have been normalized in terms of object-side focal length. The coefficients C_s and C_c have been given considerable attention since they are the two most important aberrations in electron optical systems.

3.5.1 Object-side relative spherical aberration coefficient

The relative spherical aberration coefficient has been computed as a function of the voltage ratio $\frac{V_2}{V_1}$ for various values of the separation distance **s** and at constant value of both current-turn NI and lens length L under infinite magnification condition. The trajectories in figure (3.13) have been used for

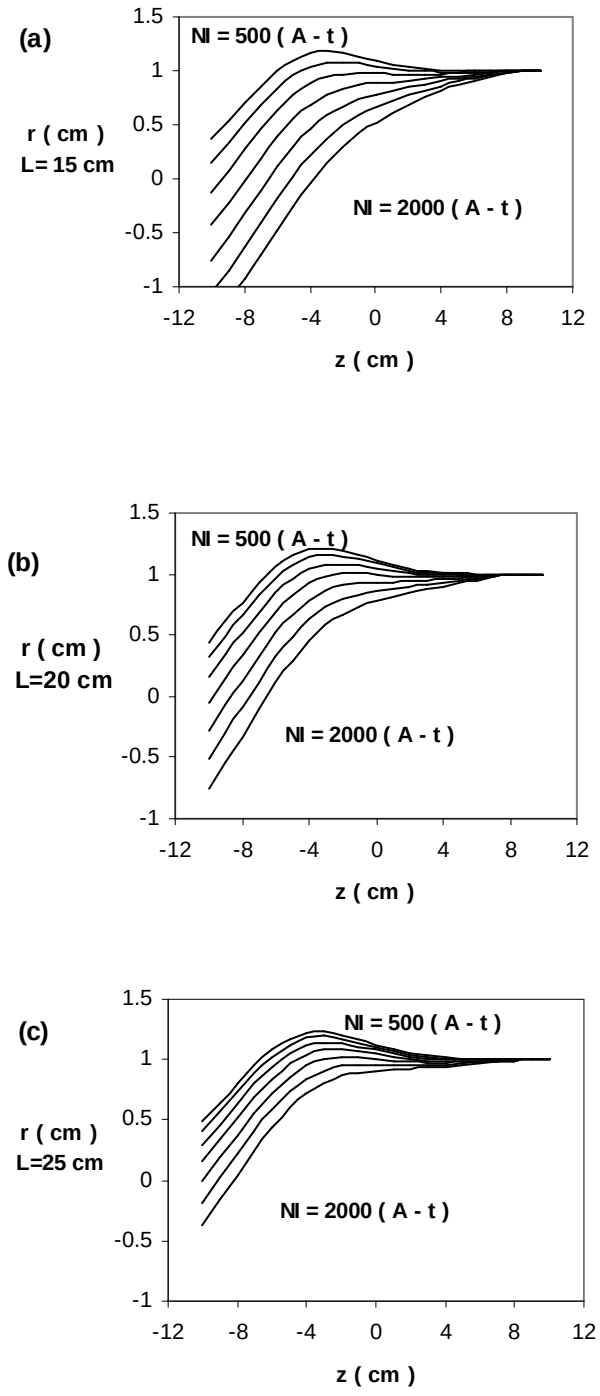

Figure 3.13. The electron beam trajectory in Gabor lens under infinite magnefication condition at various values of lens length L and current-turn NI and constant value of voltage ratio $\frac{V_2}{V_1}$ *= 8 and separation distance* $\boldsymbol{s}$ *=8 cm.*

computing the relative spherical aberration coefficient at the values of **s** = 2, 5 and 8 cm.

Figure (3.14) shows the variation of $\frac{C_{so}}{f_o}$ with $\frac{V_2}{V_1}$ for different values of the separation distance **s**. The values of NI and L are constant at 1250 A-t and 20 cm respectively. In general the values of $\frac{C_{so}}{f_o}$ are small from the electron-optics of view, even for low value of $\frac{V_2}{V_1}$. There are minima values for $\frac{C_{so}}{f_o}$ as shown in Table (3.5). One can observe from the Table that there are two minima values, when **s** = 2 and 5 cm respectively, and there is no minimum value when **s** = 8 cm. The values of $\frac{C_{so}}{f_o}$ are electron-optically acceptable, therefore there is no need to take high value for the voltage ratio $\frac{V_2}{V_1}$.

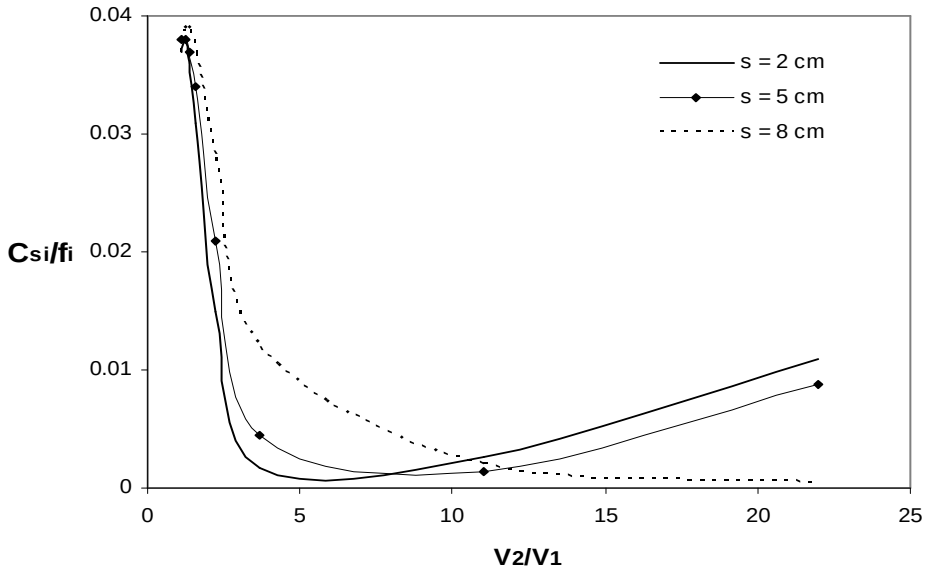

Figure 3.14. The object-side relative spherical aberration coefficient $\frac{C_{so}}{f_o}$ *as a function of the voltage ratio* $\frac{V_2}{V_1}$ *at various values of the separation distance* **s** *and at constant current-turn NI = 1250 (A – t) and lens length L = 20 cm*

Table (3.5). The minima values of the object-side relative spherical aberration coefficient and the corresponding voltage ratio $\frac{V_2}{V_1}$ *for different values of the separation distance* ***s*** *(NI = 1250 A-t, L = 20 cm)*

s (cm)	$\left(\frac{C_{so}}{f_o}\right)_{\min}$	f_i (cm)	$\frac{V_2}{V_1}$
2	0.0012	16.3	6
5	0.00139	14.6	8

The object-side relative spherical aberration coefficient $\frac{C_{so}}{f_o}$ has been studied as a function of current-turn NI for different values of lens length, and at constant values of both voltage ratio $\frac{V_2}{V_1}$ = 8 and separation distance **s** = 8 cm, as shown in figure (3.15). One can observe from the figure that the relative spherical aberration coefficient $\frac{C_{so}}{f_o}$ have small values $\frac{C_{so}}{f_o}$ increases with increasing lens length L.

$\frac{C_{so}}{f_o}$ have minima values as shown in Table (3.6). These minima values are very small, therefore there is no need to increase the current-turn NI, or even lens length, since the high value for $\frac{C_{so}}{f_o}$ are electron-optically are acceptable.

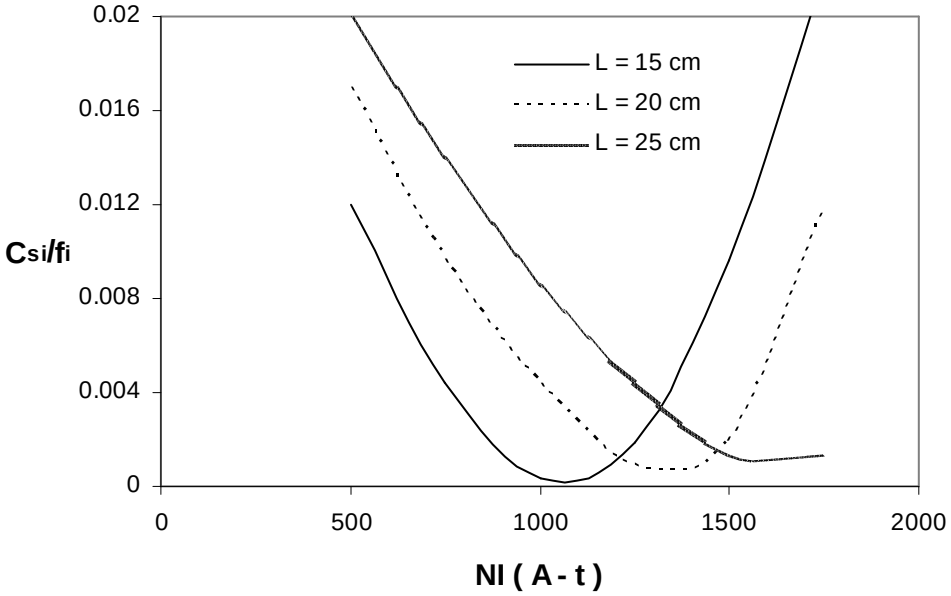

Figure 3.15. The object-side relative spherical aberration coefficient $\frac{C_{so}}{f_o}$ *as a function of the current-turn NI at various values of lens length L and at constant voltage ratio* $\frac{V_2}{V_1}$ *= 8 and separation distance* ***s*** *= 8 cm.*

Table (3.6). The minima values of the object-side relative spherical aberration coefficient and the corresponding current-turn NI for different values of the lens length L ($\frac{V_2}{V_1}$ *= 8,* ***s*** *= 8 cm).*

L (cm)	$\left(\frac{C_{so}}{f_o}\right)_{\min}$	f_i (cm)	NI (A-t)
15	0.00037	14.3	1100
20	0.00092	15.2	1400

3.5.2 Object-side relative chromatic aberration coefficient

The relative chromatic aberration coefficient $\frac{C_{co}}{f_o}$ in the object-side is shown in figure (3.16) as a function of the voltage ratio $\frac{V_2}{V_1}$ under infinite magnification condition, and for different values of the separation distance **s**. The values of the relative chromatic aberration coefficient $\frac{C_{co}}{f_o}$ in general are low, even if one increases the voltage ratio $\frac{V_2}{V_1}$ or increase the separation distance **s.**

The relative chromatic aberration coefficient has minima values as shown in the Table (3.7). This table shows that when **s** = 5 and 8 cm the minima values of the relative chromatic aberration coefficient approximately equal and occurred at the same value of the voltage ratio $\frac{V_2}{V_1}$ = 6, while when **s** = 2 cm the value of the relative chromatic aberration coefficient approximately half the value of that when **s** = 5 cm, therefore, it is preferable to operate the lens under the condition **s** = 2 cm especially, the voltage ratio $\frac{V_2}{V_1}$ doesn't increase very much.

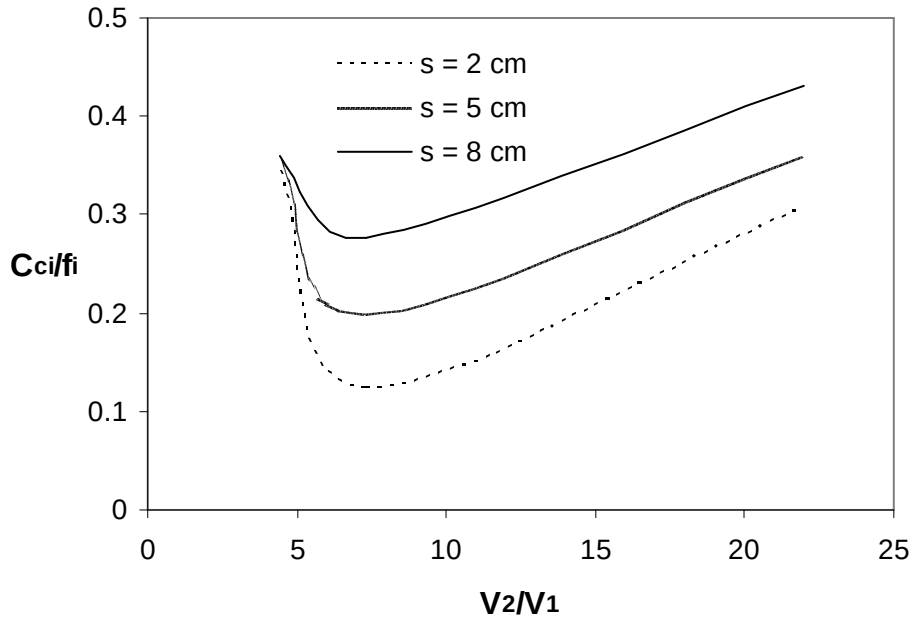

Figure 3.16. The object-side relative chromatic aberration coefficient $\frac{C_{co}}{f_o}$ *as a function of the voltage ratio* $\frac{V_2}{V_1}$ *at various values of the separation distance* ***s*** *and at constant current-turn NI = 1250 (A – t) and lens length L = 20 cm.*

Table (3.7). The minima values of the object-side relative chromatic aberration coefficient and the corresponding voltage ratio $\frac{V_2}{V_1}$ *for different values of the separation distance* ***s*** *(NI = 1250 A-t, L = 20 cm).*

s (cm)	$\left(\frac{C_{ci}}{f_i}\right)_{\min}$	$\frac{V_2}{V_1}$
2	0.125	7.33
5	0.2	6
8	0.277	6

Under infinite magnification condition the object-side relative chromatic aberration coefficient $\frac{C_{co}}{f_o}$ has been studied as a function of the current-turn NI for various values of the lens length L, and at constant values of both voltage ratio $\frac{V_2}{V_1}$ = 8 and separation distance **s** = 8 cm. Figure (3.17) shows that the values of the relative chromatic aberration are acceptable from the electron-optical point of view. Although the behaviors of the curves in figure (3.17) are different, but one can expect that if the current-turns NI increases (greater than 2000 A-t) the relative chromatic aberration coefficient have the same behavior for the three lens lengths. The relative chromatic aberration coefficients have minima values for each value of the lens length as shown in Table (3.8).

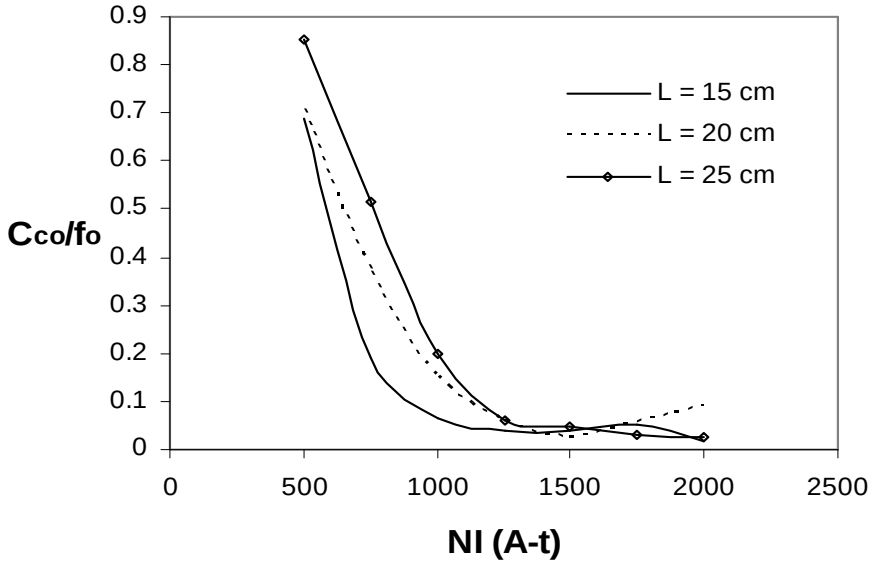

Figure 3.17. The object-side relative chromatic aberration coefficient $\frac{C_{co}}{f_o}$ *as a function of the current-turn NI at various values of the lens length L and at constant voltage ratio* $\frac{V_2}{V_1}$ *= 8 and separation distance* ***s*** *= 8 cm.*

*Table (3.8). The minima values of the object-side relative chromatic aberration coefficient and the corresponding current-turn NI for different values of the lens length L ($\frac{V_2}{V_1}$ = 8, **s** = 8 cm).*

L (cm)	$\left(\frac{C_{ci}}{f_i}\right)_{\min}$	NI (A-t)
15	0.038	1250
20	0.024	1500

3.5.3 Object-side focal length

The object-side focal length of an electrostatic and magnetic lens can be determined from the following equation **[Myers.l.M 1939]**:

$$f_o = \frac{1}{r'(z_o)} \quad \text{..... ....} \quad (3.4)$$

Under infinite magnification condition, the object-side focal length f_o of Gabor lens are computed from equation (3.3) by replacing V_2 by V_1 (first electrode voltage), as a function of the voltage ratio $\frac{V_2}{V_1}$ as shown in figure (3.18) for different values of the separation distance **s**, and at constant values of both the current-turn NI = 1250 (A-t) and lens length L = 20 cm, Figure (3.18) shows that f_o decreases with increasing voltage ratio $\frac{V_2}{V_1}$ and increases with increasing the separation distance **s**.

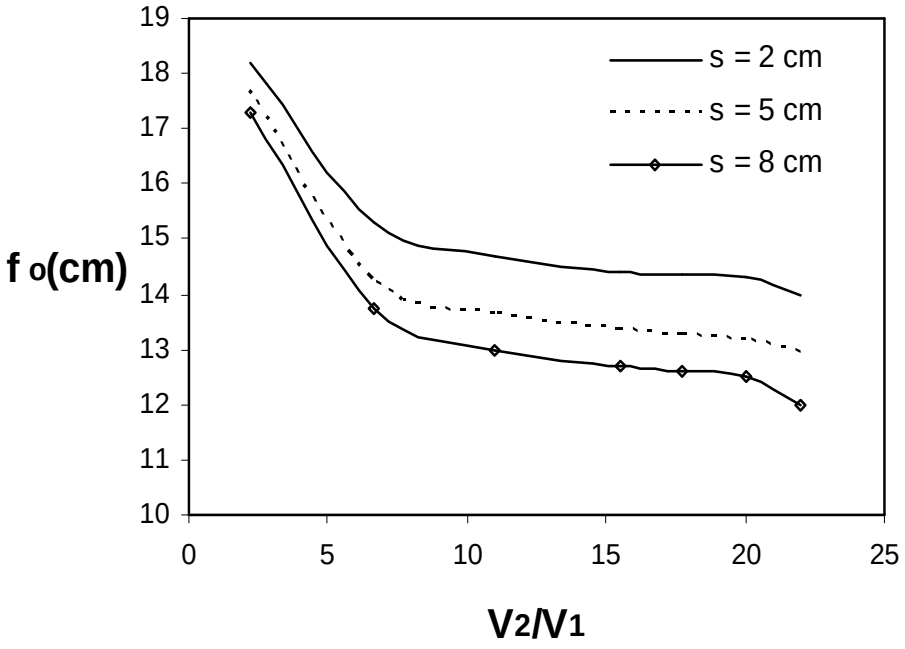

Figure 3.18. The object-side focal length as a function of the voltage ratio $\frac{V_2}{V_1}$ *at various values of the separation distance* ***s*** *and at constant value of both current-turn NI = 1250 (A-t) and lens length L = 20 cm.*

Figure (3.19) shows that the variation of the object-side focal length f_o as a function of NI at various values of the lens length L and at constant values of both the voltage ratio $\frac{V_2}{V_1}$ = 8 and separation distance **s** = 8 cm. It is seen that f_o decreases with increasing NI, this is due to the increase of the lens refractive power with increasing magnetic field. Figure (3.19) shows also that the object-side focal length f_o increases with increasing the lens length L.

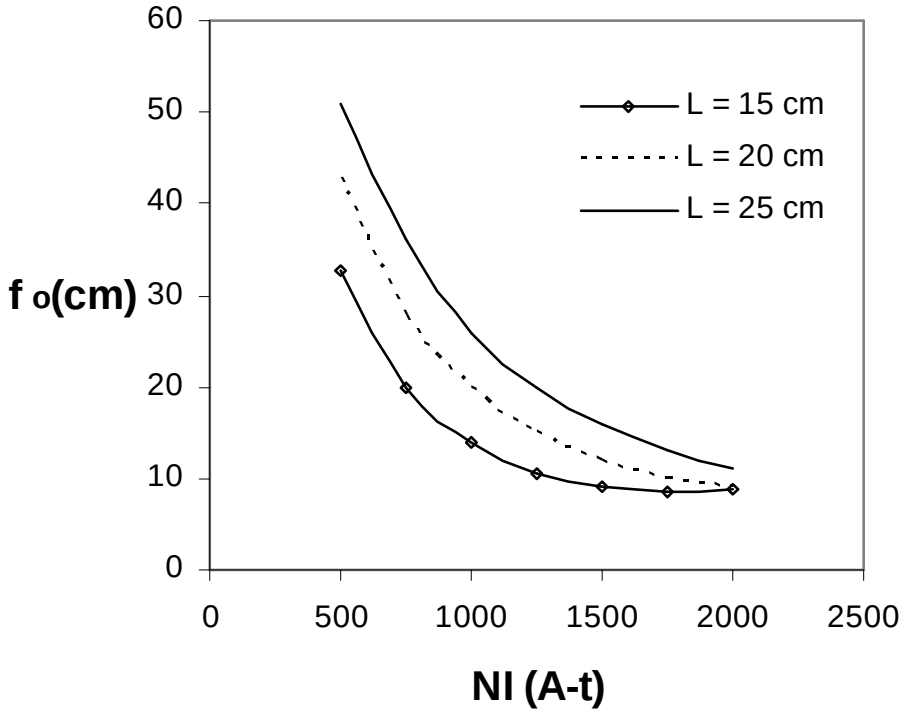

Figure 3.19. The object-side focal length as a function of the current-turn NI at various values of the lens length L and at constant values of both the voltage ratio $\frac{V_2}{V_1} = 8$ *and separation distance s = 8 cm.*